A Monolithic 3D Magnetic Sensor in 65nm CMOS with <10μT$_{rms}$ Noise and 14.8μW Power

Saransh Sharma[1], Hayward Melton[1], Liliana Edmonds[2], Olivia Addington[1], Mikhail Shapiro[1], Azita Emami[1]

[1]California Institute of Technology, Pasadena, CA

[2]Massachusetts Institute of Technology, Cambridge, MA

2023 IEEE Custom Integrated Circuits Conference (CICC) | 979-8-3503-9948-6/23/$31.00 ©2023 IEEE | DOI: 10.1109/CICC57935.2023.10121313

Magnetic sensors have become increasingly ubiquitous as they constitute an integral part of several fast-growing sectors such as automotive, navigation, robotics, medical devices and consumer electronics [1]-[6]. Due to their compatibility with the standard CMOS process, Hall magnetic sensors are widely used. However, one of the key challenges of CMOS-based Hall sensors is their relatively low sensitivity, which is inevitable given the low Hall coefficient of Si. For better sensitivity, Hall sensors are biased at higher current levels which hinders their widescale use in low-power bioelectronics and other power-constrained applications. Another challenge is the difficulty in implementing high-sensitivity vertical Hall elements in planar CMOS processes for 3D sensing. This is often overcome by using ferromagnetic materials that require additional and expensive steps during fabrication, thus increasing the cost [2][3].

We present a new 3D magnetic sensor that is fully CMOS compatible and achieves high sensitivity with only μW-level power. Though the sensor can be used for a variety of applications that require AC field sensing, it is particularly useful for biomedical applications - tracking catheters and guidewires during endovascular procedures, minimally invasive surgeries, targeted radiotherapy, and for use as fiducial markers during preoperative planning. Although coil-based magnetic sensors have been reported by NDI Aurora for electromagnetic tracking clinically [5], they are not CMOS-integrated, are at least several mm long, and lack the capability for wireless operation, thus limiting their use. In this work, the proposed magnetic sensor is employed for 3D tracking of catheters using the magnetic field gradient based spatial encoding scheme [5]. Planar electromagnetic coils are used for generating 3D field gradients that encode each spatial point uniquely, enabling 3D localization and tracking of the sensor in the field-of-view (FOV). When powered by a DC current, the Z-gradient coil (Fig.1) produces a decaying magnetic field magnitude ($\mathrm{B_0}$) along the Z-axis, resulting in the Z gradient. When powered by an AC current, the same gradient can be generated with an additional feature of exhibiting a sinusoidal variation at each point (Fig.1). X and Y axis gradients can be generated similarly.

Our sensor is composed of three orthogonal and highly dense on-chip coils that produce an induced electromotive force (EMF) in response to the AC magnetic field along each coil's axis. Since the EMF is proportional to both the magnitude and frequency of the field, AC gradients can result in higher signal levels without increasing the current in the gradient coils, resulting in higher power-efficiency. The 3D sensing coils are implemented using the available metal stack in the 65nm CMOS process. For sensing the in-plane components of the field, we need coils in the X and Y planes that are orthogonal to the chip's plane (Z). Realizing such coils is difficult due to lack of any dedicated metal layers in these planes in standard CMOS processes. In order to solve this problem, we realized the X/Y sensor coils by using the interconnect vias as part of the coil structure (Fig.1). To increase the coupling, we followed minimum design-rule-check (DRC) for both width and spacing for each metal to realize highly dense coils. An inherent challenge is the low height from M1 to AP (<20μm in 65nm) which cannot be changed. To alleviate that, we adopted two techniques: (i) the length (1.45mm) is kept much larger than the coil height; and (ii) multiple coil spirals are cascaded to increase the effective coupling area. The large number of spirals come at the cost of an increased coil resistance ($\mathrm{R_{Coil}}$) and area. Higher $\mathrm{R_{Coil}}$ leads to a higher noise floor, which necessitates the design of a low-noise front-end circuitry to achieve a high SNR. To mitigate the area penalty, the active Si area beneath the coils can be used for other on-chip components. The Z sensor coil is implemented in the plane of the chip as a multi-layer spiral (M1 to AP).

An overview of the processing circuit blocks is shown in Fig.1. $\mathrm{R_{Coil}}$ introduces a wideband noise of $\sqrt{4\mathrm{kTR}}$, which can be limited to $\sqrt{\mathrm{kT/C}}$ using $\mathrm{C_{Sense}}$. However, $\mathrm{C_{Sense}}$ cannot be arbitrarily large since the RC lowpass frequency should be higher than the EMF signal's target frequency of 500Hz. The processing circuitry is designed to handle 100Hz-1kHz of EMF and the AC power source used for the gradient coils supports 40-500Hz. $\mathrm{R_{Coil}}$ results in a thermal noise floor of 364nV/$\sqrt{\mathrm{Hz}}$ and 300nV/$\sqrt{\mathrm{Hz}}$ for the X/Y and Z sensors respectively. The X/Y sensors generate 660nV while the Z sensor generates 40μV of EMF in response to a 10μT field, which is the desired magnetic field resolution to achieve 500μm of mean localization accuracy. Since the X/Y sensors' output is close to their thermal noise floor, it is imperative to design the front-end instrumentation amplifier (IA) with 8-10x lower input-referred noise (IRN) floor. The IA is implemented in a fully-differential closed-loop architecture and is capacitively coupled to the input to avoid DC offsets and low-frequency noise (Fig.2). Pseudo-resistors are used in the feedback path to provide a GΩ-level impedance, which is needed for the high-pass corner frequency to be within 10-100Hz. The $\mathrm{G_{m1}}$ block is implemented as a cascade of two current-reuse stages. The next block is a bandpass filter (BPF) to eliminate the excessive out-of-band noise and improve the SNR (Fig.2). The programmable gain amplifier (PGA) amplifies the EMF signal for the ADC to process (Fig.2). It has a 3-bit tunable gain to accommodate the varying range of EMF throughout the FOV. To extract the peak magnitudes from the outputs of the PGA, a differential peak detect and hold (PDH) circuit is implemented (Fig.2). The outputs of the PDH are fed to a 12-bit SAR ADC (Fig.3). EM simulations are conducted to study the effect of human tissue, frequency variation and other non-idealities on the mutual inductance M (Fig.3).

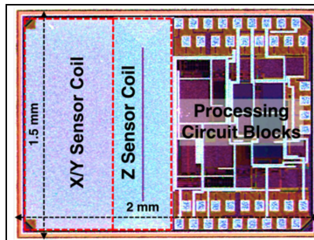

Die micrograph.

Measurement results of the sensor are shown in Fig.4 and Fig.5. The IA's IRN is <40nV/$\sqrt{\mathrm{Hz}}$ around the EMF signal frequency. The output of the PGA is ≈0.5V for a typical mV-level input, resulting in 72dB SNR. The total integrated noise for the X/Y sensors is 8mV$_{rms}$ and for the Z sensor is 1mV$_{rms}$, which translates to a raw magnetic noise of 64μT$_{rms}$ and 8μT$_{rms}$ respectively. 40 consecutive measurements are averaged to reduce the noise to 9.8μT$_{rms}$ (X/Y) and 1.2μT$_{rms}$ (Z), resulting in an update rate of 25Hz. The linearity error for both the sensor types is <0.2% in a range of $\pm$10mT. To demonstrate tracking and navigation capabilities for clinical applications, the sensor is enclosed in the tip of a 12-french catheter (Fig.5). To reduce the fabrication cost of the prototype chips, Y sensor is realized using the X sensor of another identical chip by orthogonal placement on a flex PCB. Two such catheter-enclosed devices are submerged in a tissue phantom (placed on top of the gradient coils) to perform relative tracking. The tracking error is determined by the total noise of the 3D sensor (ΔB) and the local magnetic field gradient (G). The measured error varies from a mean value of 350μm (high G FOV) to 800μm (low G FOV), while <1mm throughout the FOV (Fig.5). The comparison table (Fig.6) shows that our sensor is the first of its kind to achieve 3D magnetic sensing using three orthogonal on-chip coils in a standard CMOS process. By employing the technique of EMF induction in passive coils, the sensor does not require any power to operate. The processing circuitry consumes 14.8μW of total power which is orders of magnitude smaller than prior works [1]-[6].

References:

[1] J. Jiang *et al.*, "Multipath Wide-Bandwidth CMOS Magnetic Sensors," JSSC, 2017.

[2] M. Kashmiri *et al.*, "27.9 A 200kS/s 13.5b integrated-fluxgate differential-magnetic-to-digital converter with an oversampling compensation loop for contactless current sensing," ISSCC, 2015.

[3] C. Schott *et al.*, "CMOS Single-Chip Electronic Compass With Microcontroller," JSSC, 2007.

[4] S. Sharma *et al.*, "20.4 3D Surgical Alignment with 100μm Resolution Using Magnetic-Field Gradient-Based Localization," ISSCC, 2020.

[5] S. Sharma *et al.*, "Wireless 3D Surgical Navigation and Tracking System With 100μm Accuracy Using Magnetic-Field Gradient-Based Localization," TMI, 2021.

[6] M. Monge *et al.*, "Localization of microscale devices in vivo using addressable transmitters operated as magnetic spins," NBME, 2017.

979-8-3503-9948-6/23/$31.00 ©2023 IEEE

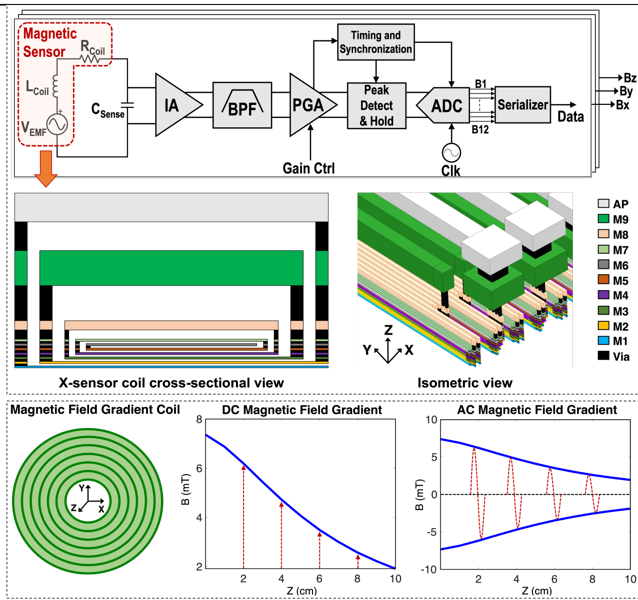

Fig. 1: 3D magnetic sensor overview and DC vs AC gradients.

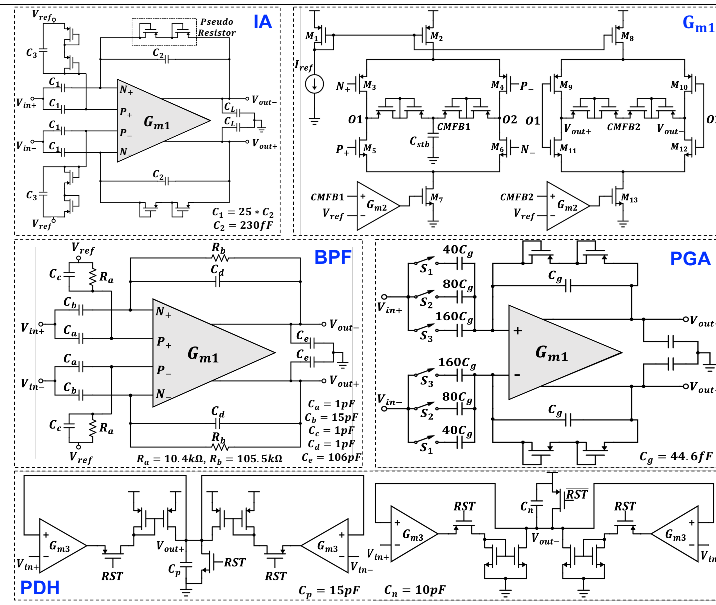

Fig. 2: Circuit schematics of the IA, G_{m1}, BPF, PGA and PDH.

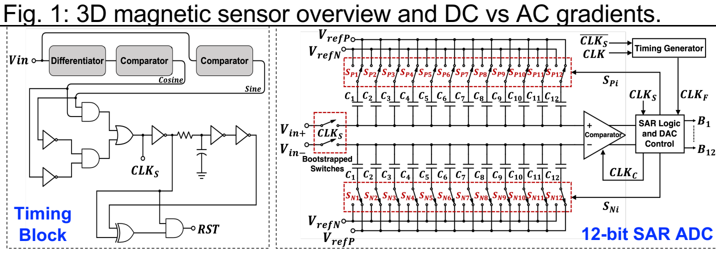

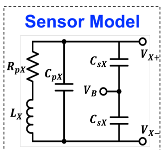

Component	Specification
L_X, L_Z	<100μH
R_{pX}	8MΩ
R_{pZ}	5.4MΩ
C_{pX}	52pF
C_{pZ}	36pF
C_{sX}, C_{sZ}	1pF
V_B	600mV

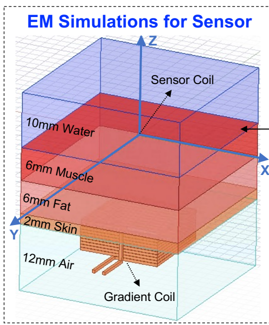

Environment	Mutual Inductance (nH) X/Y	Mutual Inductance (nH) Z
Air	1.401	87.84
Fresh water (0.01 S/m)	1.395	87.55
Sea water (4 S/m)	1.408	87.98
Tissue model	1.415	88.46

Frequency (Hz)	Mutual Inductance (nH) X/Y	Mutual Inductance (nH) Z
100	1.405	87.97
250	1.405	87.97
500	1.405	87.97
750	1.405	87.97
1000	1.405	87.97

Fig. 3: Circuit schematic of the Timing-block and ADC (top); sensor model and front-end (bottom-left); EM simulations for mutual inductance under different environment/frequency (bottom-right).

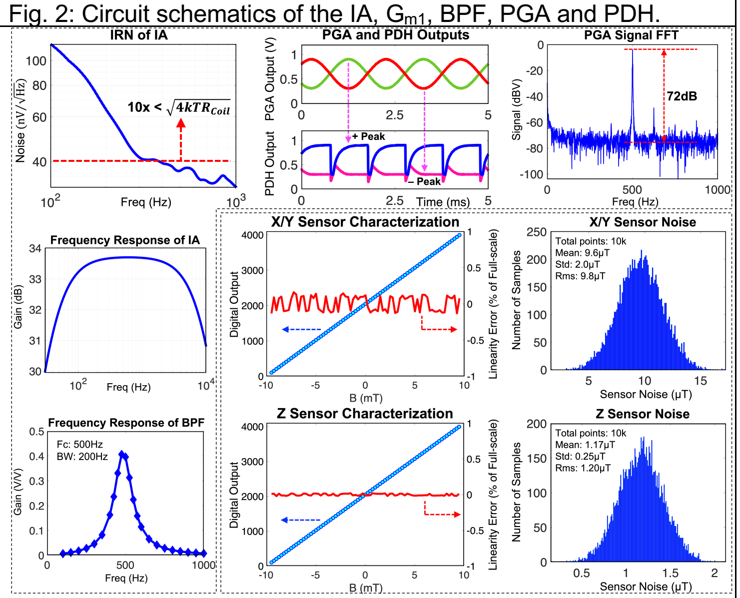

Fig. 4: Measurement results showing the IRN, frequency response, time-domain waveforms, sensor characterization and noise.

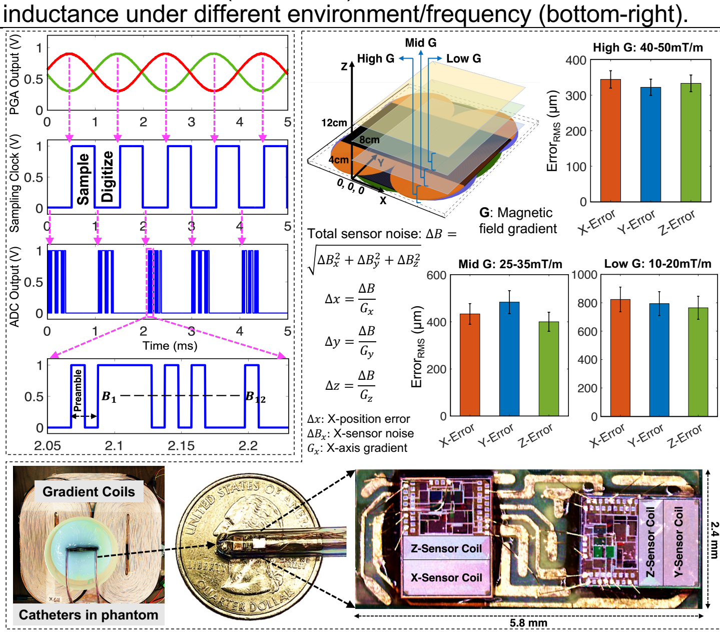

Fig. 5: Measurement results of ADC and 3D catheter localization.

	This work	ISSCC 2020 [4]	NBME 2017 [6]	JSSC 2017 [1]	ISSCC 2015 [2]	JSSC 2007 [3]
Sensing Mechanism	**EMF Induction**	Hall Effect	Hall Effect	Hall Effect + EMF Induction	Fluxgate	Hall Effect
Sensing Dimensions	**3D**	3D	1D	1D	2D	3D
CMOS Technology	**Yes (65nm CMOS)**	No	Yes (0.18μm CMOS)	Yes (0.18μm CMOS)	Yes (0.6μm CMOS)	Yes (0.35μm CMOS)
Ferromagnetic Material	**No**	N.R.	No	No	Yes	Yes
Sensor Noise (X, Y, Z)	**9.8μT_{rms} (X, Y) 1.2μT_{rms} (Z) ***	5μT_{rms} (X, Y, Z)	625μT (Z)	210μT_{rms}	0.2μT_{rms}	0.1μT (X, Y) 0.6μT (Z) &&
DC Offset	**No**	Yes	Yes	Yes (40μT)	Yes (0.9μT)	Yes (1.5μT) &&
Range	**±10mT**	±36mT	40-170mT	±7.8mT	±1.32mT	±200μT
Power	**14.8μW**	1mW	339μW	13.86mW #	280mW #	30mW
Supply Voltage	**1.2V**	2.5V	1.8V	1.8V	5V	2.2 – 3.6V
Update Frequency	**25Hz ***	7Hz	763Hz	<3MHz ##	<15kHz &	11.76Hz $
B-field Frequency	**100 – 1kHz**	DC	DC	DC – 3MHz ##	DC – 75kHz ##	DC
Digitization	**Yes (12-bit SAR ADC)**	Yes (16-bit ADC)	Off-chip	No	Yes (13.5-bit ADC)	Yes (12-bit ΣΔ ADC)
Device Dimensions	**4mm^2 ****	108x68mm^2	1.8x1.2mm^2	3.5x2.5mm^2	9.8mm^2	2.3x2.8mm^2

* Obtained by averaging 40 consecutive samples
** Estimated for a single 3D sensing chip based on the current prototype measuring 3mm^2
& Calculated from the ADC sample rate (200kS/s) and ENOB (13.5)
&& Calculated from the reported value in LSB/μT
\# Calculated from the reported current and voltage
\## Calculated from the reported sensor bandwidth
$ Calculated from the reported refresh time
N.R. – Not reported

Fig. 6: Comparison with state-of-the-art. Our CMOS-integrated 3D magnetic sensor has the lowest reported power, <10μT_{rms} noise, ±10mT range, and immunity to DC offsets and low-F noise.